Eigenstate Thermalization in Long-Range Interacting Systems

Shoki Sugimoto,[1,*] Ryusuke Hamazaki,[2] and Masahito Ueda[1,3]
[1]*Department of Physics, The University of Tokyo, 7-3-1 Hongo, Bunkyo-ku, Tokyo 113-0033, Japan*
[2]*Nonequilibrium Quantum Statistical Mechanics RIKEN Hakubi Research Team, RIKEN Cluster for Pioneering Research (CPR), RIKEN iTHEMS, Wako, Saitama 351-0198, Japan*
[3]*RIKEN Center for Emergent Matter Science (CEMS), Wako, Saitama 351-0198, Japan*

(Received 24 November 2021; revised 27 March 2022; accepted 16 June 2022; published 14 July 2022)

Motivated by recent ion experiments on tunable long-range interacting quantum systems [Neyenhuis *et al.*, Sci. Adv. **3**, e1700672 (2017)], we test the strong eigenstate thermalization hypothesis for systems with power-law interactions $\sim 1/r^\alpha$. We numerically demonstrate that the strong eigenstate thermalization hypothesis typically holds, at least for systems with $\alpha \geq 0.6$, which include Coulomb, monopole-dipole, and dipole-dipole interactions. Compared with short-range interacting systems, the eigenstate expectation value of a generic local observable is shown to deviate significantly from its microcanonical ensemble average for long-range interacting systems. We find that Srednicki's ansatz breaks down for $\alpha \lesssim 1.0$, at least for relatively large system sizes.

DOI: 10.1103/PhysRevLett.129.030602

Introduction.—Long-range interacting systems show a number of unique phenomena [1–4], such as negative heat capacity [5,6], anomalous propagation of correlations [7–12], and prethermalization [13–17]. Isolated quantum systems with long-range interactions have been realized in trapped ion systems [18], Rydberg atom arrays [19], and quantum gases coupled to optical cavities [20]. The dynamic [13,14,21,22] and thermodynamic [9,23,24] properties of these systems have also been investigated. In particular, trapped ion systems offer an ideal platform for the study of isolated quantum systems with long-range interactions $\sim 1/r^\alpha$, where the exponent α can be tuned from 0 to 3 by a spin-dependent optical dipole force [23,25–31].

Prethermalization of a long-range nonintegrable quantum system without disorder was experimentally observed [22], but complete thermalization was not observed in an experimentally accessible time. This appears inconsistent with the strong eigenstate thermalization hypothesis (ETH) [32–34], which states that an expectation value $O_{\gamma\gamma}$ of a physical observable $\hat{O}$ for *every* energy eigenstate $|E_\gamma\rangle$ of a quantum many-body Hamiltonian agrees with its microcanonical ensemble average in the thermodynamic limit [35–44]. We formulate this statement as [45]

$$\Delta_\infty := \frac{\max |O_{\gamma\gamma} - \langle \hat{O} \rangle^{\mathrm{mc}}_{\delta E}(E_\gamma)|}{\eta_O} \overset{N\to\infty}{\to} 0, \tag{1}$$

where η_O is the spectral range of $\hat{O}$ defined as the difference between the maximum and minimum eigenvalues of $\hat{O}$, and $\langle \hat{O} \rangle^{\mathrm{mc}}_{\delta E}(E_\gamma)$ is the microcanonical average of $\hat{O}$ in an energy shell $\mathcal{H}_{E_\gamma,\delta E}$ centered at E_γ with a sufficiently small width $2\delta E$. The strong ETH has numerically been verified to hold for various short-range interacting systems [45–52]. However, little is known about the validity of the strong ETH in long-range interacting systems except for a few specific models [38,53,54].

In this Letter, we test the typicality of the strong ETH for spin systems with power-law interactions $\sim 1/r^\alpha$ by introducing an "ensemble" of such systems. Our result is based on numerical diagonalization, since analytically addressing the strong ETH is extremely difficult due to a chaotic nature of energy eigenstates satisfying the ETH [34,55] and the few-body constraint of realistic operators. We find that the strong ETH typically holds, at least for $\alpha \geq 0.6$ in one dimension. For $\alpha \leq 0.5$, we find no evidence in support of the strong ETH for system size up to 20 spins relevant to trapped-ion experiments [9,10,22,23]. We also test Srednicki's ansatz [56], which states that (i) the deviation $\delta O_{\gamma\gamma} := O_{\gamma\gamma} - \langle \hat{O} \rangle^{\mathrm{mc}}_{\delta E}(E_\gamma)$ behaves like a random variable satisfying

$$\mathcal{E}[\delta O_{\gamma\gamma}] = 0, \qquad \mathcal{S}[\delta O_{\gamma\gamma}] = e^{-\frac{S(E_\gamma)}{2}} f(E_\gamma), \tag{2}$$

where $\mathcal{E}$ and $\mathcal{S}$ denote the mean and the standard deviation, respectively, S is the thermodynamic entropy, f is a smooth function, and (ii) the distribution of $\delta O_{\gamma\gamma}$ is Gaussian [49,52,57–61]. We find that both (i) and (ii) typically break down for $\alpha \lesssim 1.0$, at least for relatively large system sizes. These results imply the presence of an intermediate regime $0.5 \lesssim \alpha \lesssim 1.0$ in which the strong ETH typically holds but Srednicki's ansatz breaks down.

Our results should be distinguished from previous works concerning typical properties of Gaussian random matrices

[32,62,63], banded random matrices [64,65], and k-body embedded random matrices [66–68]. These works do not consider correlations between off-diagonal elements due to interactions, and it is unclear how these correlations affect the typicality of the strong ETH [45,69]. Our work incorporates such nontrivial correlations by explicitly constructing an ensemble of operators with long-range interactions.

Setup.—We consider a one-dimensional spin-1/2 chain of length N subject to periodic boundary condition. We denote the local Hilbert space on each site by $\mathcal{H}_{\mathrm{loc}}$ with $d_L := \dim \mathcal{H}_{\mathrm{loc}} (= 2)$, the space of all Hermitian operators acting on a Hilbert space $\mathcal{H}$ by $\mathcal{L}(\mathcal{H})$, and an orthonormal basis of $\mathcal{L}(\mathcal{H}_{\mathrm{loc}})$ by $\{\hat{\sigma}^{(p)}\}$ [70]. In numerical calculations, we set $\hat{\sigma}^{(0)} := \hat{I}$ and $\hat{\sigma}^{(p)}$ $(p = 1, 2, 3)$ to be the Pauli operators. For each α, N, and two-body operator $\hat{h} \in \mathcal{L}(\mathcal{H}_{\mathrm{loc}}^{\otimes 2})$ with $h_{pq} := [\hat{h}\hat{\sigma}^{(p)} \otimes \hat{\sigma}^{(q)}]/4$, we obtain

$$\hat{H}_N^{(\alpha)}[\hat{h}] := \sum_{p,q=1}^{d_L^2-1} h_{pq} \left[\sum_{j \neq k}^{N} \frac{\hat{\sigma}_j^{(p)} \hat{\sigma}_k^{(q)}}{(r_{jk})^{\alpha}} \right], \qquad (3)$$

where $r_{jk} := \min\{|j-k|, N-|j-k|\}$ is the minimum distance between the sites j and k under periodic boundary condition. The operator, Eq. (3), is invariant under translation $\hat{T}_N \hat{\sigma}_j^{(p)} \hat{T}_N^{\dagger} = \hat{\sigma}_{j+1}^{(p)}$ and the parity transformation $\hat{P}_N \hat{\sigma}_j^{(p)} \hat{P}_N^{\dagger} = \hat{\sigma}_{N+1-j}^{(p)}$ [71,76], and does not contain spatially random interactions or random on-site potentials. In numerical calculations, we focus on the zero-momentum and even-parity sector.

To discuss the typicality of the strong ETH and Srednicki's ansatz, we introduce a set of operators in Eq. (3) by $\mathcal{G}_N^{(\alpha)} := \{\hat{H}_N^{(\alpha)}[\hat{h}] | \hat{h} \in \mathcal{L}(\mathcal{H}_{\mathrm{loc}}^{\otimes 2})\}$. The set $\mathcal{G}_N^{(\alpha)}$ is quite general as it contains arbitrary two-body long-range operators including Ising, XYZ, Heisenberg models, etc., with arbitrary homogeneous on-site potentials and two-body long-range perturbations. We sample each h_{pq} in Eq. (3) independently from the standard normal distribution, thereby introducing a probability measure on $\mathcal{G}_N^{(\alpha)}$ [77]. For the ensemble of observables, we consider the short-range ensemble $\mathcal{G}_N^{(\infty)}$ with only nearest-neighbor and on-site terms. We investigate the typicality of the strong ETH and Srednicki's ansatz by independently sampling Hamiltonians from $\mathcal{G}_N^{(\alpha)}$ and observables from $\mathcal{G}_N^{(\infty)}$.

Finite-size scaling of the strong ETH measure.—Because of Markov's inequality, the typicality of the ETH holds if the ensemble average $\mathbb{E}_N^{(\alpha)}[\Delta_\infty]$ of the dimensionless and intensive measure Δ_∞ of the strong ETH defined in Eq. (1) vanishes in the thermodynamic limit [45]. We numerically investigate the N dependence of $\mathbb{E}_N^{(\alpha)}[\Delta_\infty]$, where α ranges from 0 to 3. Figure 1(a) shows that long-range two-body interactions make $\mathbb{E}_N^{(\alpha)}[\Delta_\infty]$ significantly larger than that for short-range interacting systems and thus disfavor the strong ETH at least for finite-size systems.

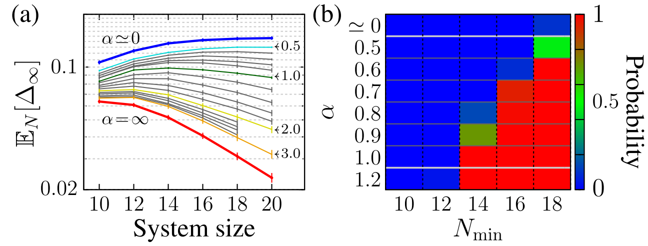

FIG. 1. (a) Ensemble-averaged strong ETH measure Δ_∞ in Eq. (1) for tunable-range interactions $\sim 1/r^{\alpha}$. To break the degeneracy in the fully connected case $(\alpha = 0)$, we set $\alpha = 0.0001$, which is small enough to capture the essential physics for $\alpha = 0$. Thin curves between $\alpha = 0.5$ and $\alpha = 1$ show the data for $\alpha = 0.6, 0.7, 0.8, 0.9$, and those between $\alpha = 1$ and $\alpha = 3$ are for $\alpha = 1.2, 1.4, \ldots, 2.8$. Each error bar shows the 80% confidence interval. (b) Probability of obtaining a sequence $\{\hat{\mathbb{E}}_N^{(\alpha)}[\Delta_\infty]\}_{N_{\mathrm{min}}}^{N_{\mathrm{max}}}$ of the estimator for $\mathbb{E}_N^{(\alpha)}[\Delta_\infty]$ such that $\hat{\mathbb{E}}_{N_{\mathrm{min}}}^{(\alpha)}[\Delta_\infty] > \hat{\mathbb{E}}_{N_{\mathrm{min}}+2}^{(\alpha)}[\Delta_\infty] > \ldots > \hat{\mathbb{E}}_{N_{\mathrm{max}}}^{(\alpha)}[\Delta_\infty]$ with $N_{\mathrm{max}} = 20$, represented by the color of the cell. This result shows that the average $\mathbb{E}_N^{(\alpha)}[\Delta_\infty]$ decreases for $\alpha \geq 0.6$ for large system size, indicating that the strong ETH typically holds for these cases (see Supplemental Material [71] for a detailed analysis). The number of samples lies between 998 and 4994 for each datum. Here, red (blue) color means that the systems are likely (unlikely) to satisfy the strong ETH.

To infer the behavior of $\mathbb{E}_N^{(\alpha)}[\Delta_\infty]$ in the thermodynamic limit, we analyze the N dependence of $\mathbb{E}_N^{(\alpha)}[\Delta_\infty]$. For Gaussian random matrices, where the few-bodiness of realistic operators is completely disregarded, the asymptotic N dependence of $\mathbb{E}_N[\Delta_\infty]$ is obtained as

$$\mathbb{E}_N^{(\mathrm{RMT})}[\Delta_\infty] \simeq C N e^{-N/N_m} \sqrt{1 - \frac{N_m}{2} \frac{\log N}{N} - \frac{N_0}{N}}, \qquad (4)$$

where C, N_m, and N_0 are constants [45]. Thus, the concave behavior in N is expected for $\mathbb{E}_N^{(\alpha)}[\Delta_\infty]$, and it is therefore important to check whether numerically obtained $\mathbb{E}_N^{(\alpha)}[\Delta_\infty]$ decreases for larger N [78].

The level of confidence that $\mathbb{E}_N^{(\alpha)}[\Delta_\infty]$ decreases with increasing N can be measured by the probability of obtaining a sequence of the estimator $\{\hat{\mathbb{E}}_{N_{\mathrm{min}}}^{(\alpha)}[\Delta_\infty], \ldots, \hat{\mathbb{E}}_{N_{\mathrm{max}}}^{(\alpha)}[\Delta_\infty]\}$ such that $\hat{\mathbb{E}}_{N_{\mathrm{min}}}^{(\alpha)}[\Delta_\infty] > \hat{\mathbb{E}}_{N_{\mathrm{min}}+2}^{(\alpha)}[\Delta_\infty] > \ldots > \hat{\mathbb{E}}_{N_{\mathrm{max}}}^{(\alpha)}[\Delta_\infty]$ in bootstrap iterations (see Supplemental Material [71] for details). Figure 1(b) shows that $\mathbb{E}_N^{(\alpha)}[\Delta_\infty]$ for $\alpha \geq 0.6$ decreases for large N [79]. Therefore, the strong ETH typically holds at least for $\alpha \geq 0.6$. For $\alpha \leq 0.5$, $\mathbb{E}_N^{(\alpha)}[\Delta_\infty]$ does not decrease within statistical errors. While this result suggests the breakdown of the strong ETH for $\alpha \leq 0.5$, we cannot exclude the possibility that $\mathbb{E}_N^{(\alpha)}[\Delta_\infty]$ vanishes in the thermodynamic limit and that the strong ETH typically holds for $0 < \alpha \leq 0.5$. Nevertheless, our results for finite-size systems are relevant to trapped-ion experiments [9,10,22,23], where systems involve several tens of ions. For the fully connected case ($\alpha = 0$), the strong ETH typically breaks down in arbitrary dimensions because permutation operators of any two neighboring sites are conserved. This result is consistent with a monotonically increasing behavior of $\mathbb{E}_N^{(\alpha)}[\Delta_\infty]$ for $\alpha \simeq 0$ in Fig. 1.

Proximity to the fully connected case.—To understand how the transition from the fully connected case to the short-range one occurs, we employ finite-size scaling to examine the level spacing ratio and the fractal dimension. We first examine the level spacing ratio [80,81] defined by

$$\tilde{r}_\gamma \coloneqq \min\left\{r_\gamma, \frac{1}{r_\gamma}\right\}, \qquad r_\gamma \coloneqq \frac{E_{\gamma+1} - E_\gamma}{E_\gamma - E_{\gamma-1}}. \tag{5}$$

The spectral average $\langle \tilde{r} \rangle$ is known to be $\langle \tilde{r} \rangle \simeq 0.602\,66$ for Gaussian unitary ensemble (GUE) and $\langle \tilde{r} \rangle \simeq 0.386\,29$ for integrable systems whose level spacing distribution is Poissonian [81].

Figure 2(a) shows the system-size dependence of the ensemble average $\mathbb{E}_N^{(\alpha)}[\langle \tilde{r} \rangle]$ for several values of α. For every ensemble examined ($\alpha \geq 0.25$), it approaches the GUE value as the system size increases. Therefore, the approximate permutation symmetry has a lesser effect for larger systems.

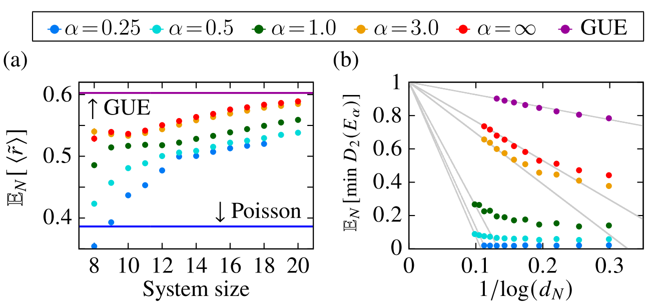

FIG. 2. (a) Ensemble average of the mean level spacing ratio $\langle \tilde{r} \rangle$ defined in Eq. (5), where the average $\langle \cdots \rangle$ is taken over the middle 10% of the spectrum. It approaches the GUE value for all α with increasing system size. (b) Ensemble average of the minimum fractal dimension with $q = 2$ for energy eigenstates of $\hat{H}_N^{(\alpha)}$ with respect to the eigenbasis of the fully connected Hamiltonian $\hat{H}_N^{(0)}$. The minimum is taken over the middle 10% of the spectrum. It approaches unity for $\alpha \geq 1.0$ with increasing d_N. Whether the data for $\alpha = 0.5$ approaches unity or converges to a smaller value is unclear. For $\alpha = 0.25$, the minimum fractal dimension shows no increase. Each gray line connects the point (0,1) and the data point with the largest d_N. The number of samples lies between 996 and 4994. Most error bars are smaller than the dot size.

This result is consistent with the one for the transverse-field Ising chain with long-range interactions [82]. However, for small α, $\mathbb{E}_N^{(\alpha)}[\langle \tilde{r} \rangle]$ approximately lies in the middle of the GUE and Poissonian values for finite system sizes up to $N = 20$. This fact indicates that the approximate permutation symmetry persists for small α in systems with a few dozens of particles.

We next evaluate the fractal dimension [83] of eigenstates of a Hamiltonian $\hat{H}_N^{(\alpha)}[\hat{h}]$ in the eigenbasis of the corresponding fully connected Hamiltonian $\hat{H}_N^{(0)}[\hat{h}]$. The fractal dimension is defined by

$$D_q(E_\beta^{(\alpha)}) \coloneqq -\frac{1}{\log d_N}\frac{1}{q-1}\log\left(\sum_{\gamma=1}^{d_N} |\langle E_\gamma^{(0)}|E_\beta^{(\alpha)}\rangle|^{2q}\right), \tag{6}$$

where $|E_\beta^{(\alpha)}\rangle$ is an eigenstate of $\hat{H}_N^{(\alpha)}[\hat{h}]$ with eigenenergy $E_\beta^{(\alpha)}$, and $\{|E_\gamma^{(0)}\rangle\}$ is the eigenbasis of $\hat{H}_N^{(0)}$ to which the eigenbasis $\{|E_\gamma^{(\alpha)}\rangle\}$ converges in the limit $\alpha \to 0$ [84]. The fractal dimension satisfies $0 \leq D_q \leq 1$, where the first equality holds if and only if $|\langle E_\gamma^{(0)}|E_\beta^{(\alpha)}\rangle|^2 = 1$ for some γ, and the second equality holds if and only if $|\langle E_\gamma^{(0)}|E_\beta^{(\alpha)}\rangle|^2 = 1/d_N$ for all γ [85].

Figure 2(b) plots the ensemble average of the minimum fractal dimension $D_2(E_\beta^{(\alpha)})$ in the middle 10% of the energy spectrum against $1/\log d_N$, where d_N is the dimension of the zero-momentum even-parity sector. For $\alpha \geq 3.0$, $D_2(E_\beta^{(\alpha)})$ approaches unity as the dimension of the Hilbert space increases, indicating that the approximate permutation symmetry disappears for sufficiently large system size. The data for $\alpha = 1.0$ also tends to approach unity, albeit slowly.

Although the fractal dimension for $\alpha = 0.5$ slightly increases for $1/\log d_N \geq 0.09$ ($N \leq 20$), its slope is not large enough to determine whether it approaches unity or converges to a smaller value. For the ensemble with $\alpha = 0.25$, $D_2(E_\beta^{(\alpha)})$ does not increase within computationally accessible system size ($N \leq 20$), suggesting that it remains small for larger system size. Thus, eigenstates of Hamiltonians with $\alpha \lesssim 0.5$ retain some resemblance to those of the fully connected Hamiltonian even for large system size. Since the eigenstates of a fully connected Hamiltonian typically violate the strong ETH, the eigenstate expectation values for $\alpha \lesssim 0.5$ are expected to deviate from the microcanonical average even for relatively large system sizes due to the proximity to the fully connected Hamiltonian.

Range of validity of Srednicki's ansatz.—We test the validity of the first part [Eq. (2)] of Srednicki's ansatz (see Supplemental Material [71] for the second). By applying Boltzmann's formula $S(E) \sim \log d_{E,\delta E}$ with $d_{E,\delta E} \coloneqq \dim \mathcal{H}_{E,\delta E}$ to Eq. (2), we obtain $\mathcal{S}[\delta O_{\gamma\gamma}] \simeq (\sqrt{d_{E_\gamma,\delta E}})^{-1} f(E_\gamma)$ [86]. We test Eq. (2) for our ensembles

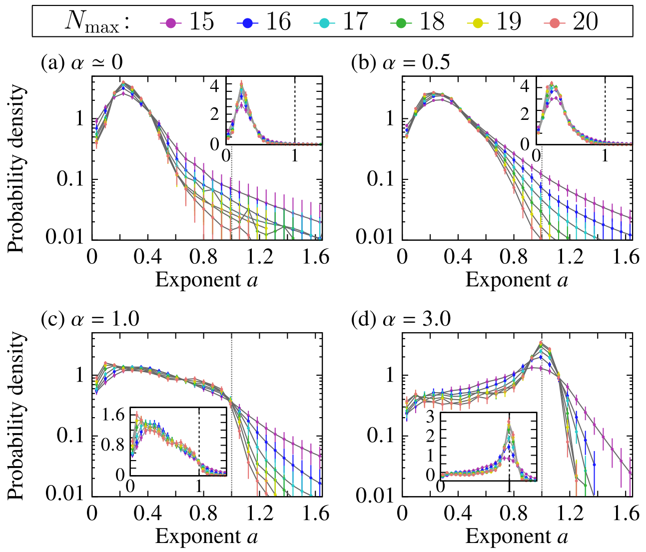

FIG. 3. Distribution of the exponent a obtained from the fitting $\hat{\mathcal{S}}^{E}_{\delta E} \propto (\sqrt{d_{E,\delta E}})^{-a}$. The inset shows the same data in linear scale. The existence of a clear peak around $a = 1$ shows that Srednicki's ansatz holds for $\alpha = 3.0$. No peak around $a = 1$ can be found for $\alpha \leq 1.0$ even for the largest available system size, indicating the breakdown of Srednicki's ansatz at least for relatively large system sizes. The number of samples lies between 1000 and 5000.

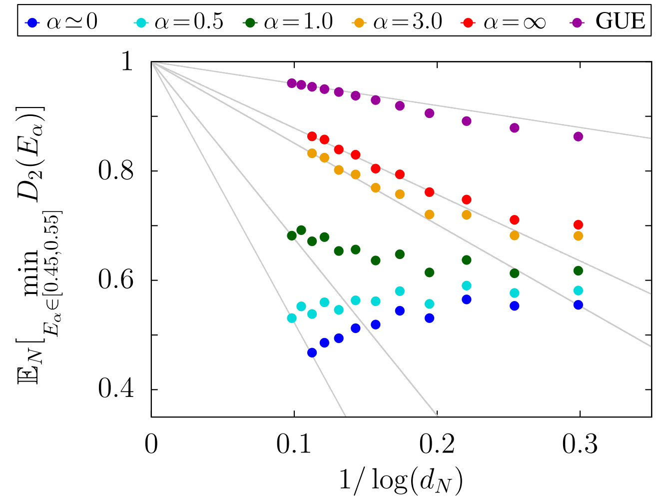

FIG. 4. Ensemble average of the minimum fractal dimension, Eq. (6), of energy eigenstates with respect to the eigenbasis of a local observable $\hat{O}$. While it approaches unity for $\alpha \geq 3.0$, it increases rather slowly for $\alpha = 1.0$ and decreases for $\alpha \leq 0.5$ as we increase $\log(d_N)$, indicating a strong correlation between long-ranged Hamiltonians and local observables. The number of samples ranges from 932 to 2000 for all data points.

by investigating the $d_{E,\delta E}$ dependence of the estimator $\hat{\mathcal{S}}^{E}_{\delta E}$ of $\mathcal{S}[\delta O_{\gamma\gamma}]|_{E_\gamma \simeq E} = \sqrt{\mathcal{E}[(\delta O_{\gamma\gamma})^2]|}_{E_\gamma \simeq E}$ defined by

$$\hat{\mathcal{S}}^{E}_{\delta E} \coloneqq \sqrt{\frac{1}{d_{E,\delta E}} \sum_{|E_\gamma\rangle \in \mathcal{H}_{E,\delta E}} (\delta O_{\gamma\gamma})^2}. \tag{7}$$

For each sample $(\hat{h}, \hat{o}) \in \mathcal{L}(\mathcal{H}_{\mathrm{loc}}^{\otimes 2}) \times \mathcal{L}(\mathcal{H}_{\mathrm{loc}}^{\otimes 2})$, we construct a Hamiltonian $\hat{H}_N^{(\alpha)}[\hat{h}]$ and an observable $\hat{O}_N^{(\infty)}[\hat{o}]$ as in Eq. (3) for various N and fit the numerically obtained $\hat{\mathcal{S}}^{E}_{\delta E}$ with a function $C(\sqrt{d_{E,\delta E}})^{-a}$ by appropriately choosing parameters C and a (note that $d_{E,\delta E}$ depends on N). The validity of this fitting is tested by comparing its mean squared residual with that of the fitting with a function $C'(\log d_{E,\delta E})^{-a'}$ (a' is a fitting parameter), which applies to the integrable case. The probability distributions of a for different α are shown in Fig. 3.

If Srednicki's ansatz holds typically, we have $a \sim 1$ with high probability; therefore, the probability distribution of a should peak around unity. To estimate finite-size effects, we restrict the available system size for the fitting of $\hat{\mathcal{S}}^{E}_{\delta E}$ with $C(\sqrt{d_{E,\delta E}})^{-a}$ to $N_{\max}$ and vary $N_{\max}$. For $\alpha = 3.0$, the probability density tends to peak around $a = 1$ and decreases for small a as $N_{\max}$ increases. We find a similar tendency for $\alpha \gtrsim 1.2$ (see Supplemental Material [71]). Therefore, the first part of Srednicki's ansatz typically holds in the thermodynamic limit for $\alpha \gtrsim 1.2$.

However, the finite-size-scaling behavior for $\alpha \leq 1$ shows no tendency for the distribution to peak around unity, indicating the breakdown of Srednicki's ansatz at least for relatively large system sizes. For small α ($\lesssim 0.5$), $C'(\log d_{E,\delta E})^{-a'}$ fits the data as well as $C(\sqrt{d_{E,\delta E}})^{-a}$. This fact indicates that the peaks of the distributions for $\alpha = 0.5$ and $\alpha \simeq 0$ in Fig. 3 are artifacts of an improper fitting to $C(\sqrt{d_{E,\delta E}})^{-a}$, which always yields a positive value of a whenever $\hat{\mathcal{S}}^{E}_{\delta E}$ decreases with increasing $d_{E,\delta E}$.

Srednicki's ansatz is based on the observation that the relationship of a quantum many-body Hamiltonian to a physical observable resembles that between two Gaussian random matrices [49]. To check this for long-range interactions, we examine the system-size dependence of the fractal dimension, Eq. (6), of eigenstates of $\hat{H}_N^{(\alpha)}$ with $\alpha \in [0, 3]$ in the eigenbasis of a local operator $\hat{O}_N^{(\infty)}$, i.e., we replace $\{|E_\gamma^{(0)}\rangle\}$ in Eq. (6) with the eigenbasis of $\hat{O}_N^{(\infty)}$. The results are shown in Fig. 4. For $\alpha \geq 3$, where the typicality of both the strong ETH and Srednicki's ansatz has been established in Ref. [45] and Fig. 3, we find that the fractal dimension approaches unity as the system size increases. However, the fractal dimension increases rather slowly for $\alpha = 1.0$ and decreases for $\alpha \leq 0.5$. This result implies a strong correlation between eigenstates of a Hamiltonian and those of a local observable when the interactions are long-ranged, invalidating the application of the conventional random matrix theory for $\alpha \lesssim 1.0$.

Conclusion.—We have found that the strong ETH typically holds for one-dimensional systems with two-body long-range interactions $1/r^{\alpha}$, at least for $\alpha \gtrsim 0.6$, which include important cases of Coulomb ($\alpha = 1$), monopole-dipole ($\alpha = 2$), and dipole-dipole ($\alpha = 3$) interactions. We have also shown that $\mathbb{E}_N^{(\alpha)}[\Delta_\infty]$ for generic two-body long-range interactions is significantly larger than that for short-range interactions. Indeed, we cannot decide whether or not the strong ETH typically holds for $\alpha \leq 0.5$ within the computationally available system sizes ($N \leq 20$). These results are directly relevant for understanding thermalization dynamics of finite-size systems realizable in experiments. We find that Srednicki's ansatz typically holds for $\alpha \gtrsim 1.2$ but typically breaks down for $\alpha \lesssim 1.0$ for computationally tractable system size. Our results reveal a region ($0.5 \lesssim \alpha \lesssim 1.0$) where the strong ETH typically holds but Srednicki's ansatz typically breaks down.

Thus, not only the experimentally investigated long-range Ising interaction [22] but also *generic* long-range interactions impede thermalization. We have studied the dynamics of long-range interacting systems from simple initial states with energy expectation values in the middle 20% of the spectrum and found that the equilibrium expectation value of a short-range observable typically deviates more from the microcanonical average for smaller α [71].

The critical value $\alpha_c = 1.0$ below which Srednicki's ansatz typically breaks down for one-dimensional systems is precisely the value below which the additivity of a physical quantity is lost. Given the importance of additivity in thermodynamics, we expect that the strong ETH and Srednicki's ansatz typically hold, at least when the range of interactions is shorter than $1/r^d$ for d-dimensional systems. It remains a challenge to clarify the relationship between the additivity and the strong ETH, and how the critical value of α changes for higher dimensions.

We are very grateful to Synge Todo and Tilman Hartwig for their help in our numerical calculation. We also thank Liu Ziyin for helpful discussions in the statistical analysis. Diagonalizations and multiplications of matrices in the numerical calculation were performed with GPU acceleration provided by the MAGMA library [96–98]. This work is was supported by KAKENHI Grants No. JP22H01152 from the Japan Society for the Promotion of Science (JSPS). S. S. was supported by Forefront Physics and Mathematics Program to Drive Transformation (FoPM), a World-leading Innovative Graduate Study (WINGS) Program, the University of Tokyo.

[*]Corresponding author.
sugimoto@cat.phys.s.u-tokyo.ac.jp

[1] T. Dauxois, S. Ruffo, E. Arimondo, and M. Wilkens, *Dynamics and Thermodynamics of Systems with Long-Range Interactions* (Springer, Berlin, Heidelberg, 2002), 10.1007/3-540-45835-2.

[2] A. Campa, T. Dauxois, and S. Ruffo, Statistical mechanics and dynamics of solvable models with long-range interactions, Phys. Rep. **480**, 57 (2009).

[3] A. Campa, T. Dauxois, D. Fanelli, and S. Ruffo, *Physics of Long-Range Interacting Systems* (Oxford University Press, New York, 2014), 10.1093/acprof:oso/9780199581931.001.0001.

[4] N. Defenu, T. Donner, T. Macrì, G. Pagano, S. Ruffo, and A. Trombettoni, Long-range interacting quantum systems, arXiv:2109.01063.

[5] M. Schmidt, R. Kusche, T. Hippler, J. Donges, W. Kronmüller, B. von Issendorff, and H. Haberland, Negative Heat Capacity for a Cluster of 147 Sodium Atoms, Phys. Rev. Lett. **86**, 1191 (2001).

[6] F. Gobet, B. Farizon, M. Farizon, M. J. Gaillard, J. P. Buchet, M. Carré, and T. D. Märk, Probing the Liquid-to-Gas Phase Transition in a Cluster via a Caloric Curve, Phys. Rev. Lett. **87**, 203401 (2001).

[7] P. Hauke and L. Tagliacozzo, Spread of Correlations in Long-Range Interacting Quantum Systems, Phys. Rev. Lett. **111**, 207202 (2013).

[8] J. Schachenmayer, B. P. Lanyon, C. F. Roos, and A. J. Daley, Entanglement Growth in Quench Dynamics with Variable Range Interactions, Phys. Rev. X **3**, 031015 (2013).

[9] P. Richerme, Z.-X. Gong, A. Lee, C. Senko, J. Smith, M. Foss-Feig, S. Michalakis, A. V. Gorshkov, and C. Monroe, Non-local propagation of correlations in quantum systems with long-range interactions, Nature (London) **511**, 198 (2014).

[10] P. Jurcevic, B. P. Lanyon, P. Hauke, C. Hempel, P. Zoller, R. Blatt, and C. F. Roos, Quasiparticle engineering and entanglement propagation in a quantum many-body system, Nature (London) **511**, 202 (2014).

[11] L. Cevolani, J. Despres, G. Carleo, L. Tagliacozzo, and L. Sanchez-Palencia, Universal scaling laws for correlation spreading in quantum systems with short- and long-range interactions, Phys. Rev. B **98**, 024302 (2018).

[12] J. T. Schneider, J. Despres, S. J. Thomson, L. Tagliacozzo, and L. Sanchez-Palencia, Spreading of correlations and entanglement in the long-range transverse Ising chain, Phys. Rev. Research **3**, L012022 (2021).

[13] M. van den Worm, B. C. Sawyer, J. J. Bollinger, and M. Kastner, Relaxation timescales and decay of correlations in a long-range interacting quantum simulator, New J. Phys. **15**, 083007 (2013).

[14] Z.-X. Gong and L.-M. Duan, Prethermalization and dynamic phase transition in an isolated trapped ion spin chain, New J. Phys. **15**, 113051 (2013).

[15] M. Marcuzzi, J. Marino, A. Gambassi, and A. Silva, Prethermalization in a Nonintegrable Quantum Spin Chain after a Quench, Phys. Rev. Lett. **111**, 197203 (2013).

[16] T. Mori, Prethermalization in the transverse-field Ising chain with long-range interactions, J. Phys. A **52**, 054001 (2019).

[17] N. Defenu, Metastability and discrete spectrum of long-range systems, Proc. Natl. Acad. Sci. U.S.A. **118**, e2101785118 (2021).

[18] R. Blatt and C. F. Roos, Quantum simulations with trapped ions, Nat. Phys. **8**, 277 (2012).
[19] A. Browaeys and T. Lahaye, Many-body physics with individually controlled rydberg atoms, Nat. Phys. **16**, 132 (2020).
[20] H. Ritsch, P. Domokos, F. Brennecke, and T. Esslinger, Cold atoms in cavity-generated dynamical optical potentials, Rev. Mod. Phys. **85**, 553 (2013).
[21] J. Smith, A. Lee, P. Richerme, B. Neyenhuis, P. W. Hess, P. Hauke, M. Heyl, D. A. Huse, and C. Monroe, Many-body localization in a quantum simulator with programmable random disorder, Nat. Phys. **12**, 907 (2016).
[22] B. Neyenhuis, J. Zhang, P. W. Hess, J. Smith, A. C. Lee, P. Richerme, Z.-X. Gong, A. V. Gorshkov, and C. Monroe, Observation of prethermalization in long-range interacting spin chains, Sci. Adv. **3**, e1700672 (2017).
[23] R. Islam, E. E. Edwards, K. Kim, S. Korenblit, C. Noh, H. Carmichael, G.-D. D. Lin, L.-M. M. Duan, C.-C. J. Wang, J. K. Freericks, and C. Monroe, Onset of a quantum phase transition with a trapped ion quantum simulator, Nat. Commun. **2**, 377 (2011).
[24] R. Islam, C. Senko, W. C. Campbell, S. Korenblit, J. Smith, A. Lee, E. E. Edwards, C.-C. J. Wang, J. K. Freericks, and C. Monroe, Emergence and frustration of magnetism with variable-range interactions in a quantum simulator, Science **340**, 583 (2013).
[25] D. Porras and J. I. Cirac, Effective Quantum Spin Systems with Trapped Ions, Phys. Rev. Lett. **92**, 207901 (2004).
[26] K. Kim, M.-S. Chang, R. Islam, S. Korenblit, L.-M. Duan, and C. Monroe, Entanglement and Tunable Spin-Spin Couplings between Trapped Ions Using Multiple Transverse Modes, Phys. Rev. Lett. **103**, 120502 (2009).
[27] J. W. Britton, B. C. Sawyer, A. C. Keith, C.-C. J. Wang, J. K. Freericks, H. Uys, M. J. Biercuk, and J. J. Bollinger, Engineered two-dimensional Ising interactions in a trapped-ion quantum simulator with hundreds of spins, Nature (London) **484**, 489 (2012).
[28] B. Yoshimura, M. Stork, D. Dadic, W. C. Campbell, and J. K. Freericks, Creation of two-dimensional Coulomb crystals of ions in oblate Paul traps for quantum simulations, Eur. Phys. J. Quantum Technol. **2**, 2 (2015).
[29] J. G. Bohnet, B. C. Sawyer, J. W. Britton, M. L. Wall, A. M. Rey, M. Foss-Feig, and J. J. Bollinger, Quantum spin dynamics and entanglement generation with hundreds of trapped ions, Science **352**, 1297 (2016).
[30] P. Richerme, Two-dimensional ion crystals in radio-frequency traps for quantum simulation, Phys. Rev. A **94**, 032320 (2016).
[31] P. W. Hess, P. Becker, H. B. Kaplan, A. Kyprianidis, A. C. Lee, B. Neyenhuis, G. Pagano, P. Richerme, C. Senko, J. Smith, W. L. Tan, J. Zhang, and C. Monroe, Non-thermalization in trapped atomic ion spin chains, Phil. Trans. R. Soc. A **375**, 20170107 (2017).
[32] J. von Neumann, Beweis des Ergodensatzes und desH-Theorems in der neuen Mechanik, Z. Phys. **57**, 30 (1929).
[33] J. M. Deutsch, Quantum statistical mechanics in a closed system, Phys. Rev. A **43**, 2046 (1991).
[34] M. Srednicki, Chaos and quantum thermalization, Phys. Rev. E **50**, 888 (1994).
[35] M. Rigol, V. Dunjko, and M. Olshanii, Thermalization and its mechanism for generic isolated quantum systems, Nature (London) **452**, 854 (2008).
[36] M. Rigol, Breakdown of Thermalization in Finite One-Dimensional Systems, Phys. Rev. Lett. **103**, 100403 (2009).
[37] G. Biroli, C. Kollath, and A. M. Läuchli, Effect of Rare Fluctuations on the Thermalization of Isolated Quantum Systems, Phys. Rev. Lett. **105**, 250401 (2010).
[38] E. Khatami, M. Rigol, A. Relaño, and A. M. García-García, Quantum quenches in disordered systems: Approach to thermal equilibrium without a typical relaxation time, Phys. Rev. E **85**, 050102(R) (2012).
[39] A. Polkovnikov, K. Sengupta, A. Silva, and M. Vengalattore, Colloquium: Nonequilibrium dynamics of closed interacting quantum systems, Rev. Mod. Phys. **83**, 863 (2011).
[40] J. Eisert, M. Friesdorf, and C. Gogolin, Quantum many-body systems out of equilibrium, Nat. Phys. **11**, 124 (2015).
[41] C. Gogolin and J. Eisert, Equilibration, thermalisation, and the emergence of statistical mechanics in closed quantum systems, Rep. Prog. Phys. **79**, 056001 (2016).
[42] L. D'Alessio, Y. Kafri, A. Polkovnikov, and M. Rigol, From quantum chaos and eigenstate thermalization to statistical mechanics and thermodynamics, Adv. Phys. **65**, 239 (2016).
[43] T. Mori, T. N. Ikeda, E. Kaminishi, and M. Ueda, Thermalization and prethermalization in isolated quantum systems: A theoretical overview, J. Phys. B **51**, 112001 (2018).
[44] J. M. Deutsch, Eigenstate thermalization hypothesis, Rep. Prog. Phys. **81**, 082001 (2018).
[45] S. Sugimoto, R. Hamazaki, and M. Ueda, Test of the Eigenstate Thermalization Hypothesis Based on Local Random Matrix Theory, Phys. Rev. Lett. **126**, 120602 (2021).
[46] M. Rigol and L. F. Santos, Quantum chaos and thermalization in gapped systems, Phys. Rev. A **82**, 011604(R) (2010).
[47] L. F. Santos and M. Rigol, Localization and the effects of symmetries in the thermalization properties of one-dimensional quantum systems, Phys. Rev. E **82**, 031130 (2010).
[48] R. Steinigeweg, J. Herbrych, and P. Prelovšek, Eigenstate thermalization within isolated spin-chain systems, Phys. Rev. E **87**, 012118 (2013).
[49] W. Beugeling, R. Moessner, and M. Haque, Finite-size scaling of eigenstate thermalization, Phys. Rev. E **89**, 042112 (2014).
[50] H. Kim, T. N. Ikeda, and D. A. Huse, Testing whether all eigenstates obey the eigenstate thermalization hypothesis, Phys. Rev. E **90**, 052105 (2014).
[51] R. Steinigeweg, A. Khodja, H. Niemeyer, C. Gogolin, and J. Gemmer, Pushing the Limits of the Eigenstate Thermalization Hypothesis Towards Mesoscopic Quantum Systems, Phys. Rev. Lett. **112**, 130403 (2014).
[52] D. Jansen, J. Stolpp, L. Vidmar, and F. Heidrich-Meisner, Eigenstate thermalization and quantum chaos in the Holstein polaron model, Phys. Rev. B **99**, 155130 (2019).
[53] E. Khatami, G. Pupillo, M. Srednicki, and M. Rigol, Fluctuation-Dissipation Theorem in an Isolated System of Quantum Dipolar Bosons after a Quench, Phys. Rev. Lett. **111**, 050403 (2013).

[54] T. Mori, Classical ergodicity and quantum eigenstate thermalization: Analysis in fully connected Ising ferromagnets, Phys. Rev. E **96**, 012134 (2017).

[55] M. V. Berry, Regular and irregular semiclassical wavefunctions, J. Phys. A **10**, 2083 (1977).

[56] M. Srednicki, The approach to thermal equilibrium in quantized chaotic systems, J. Phys. A **32**, 1163 (1999).

[57] W. Beugeling, R. Moessner, and M. Haque, Off-diagonal matrix elements of local operators in many-body quantum systems, Phys. Rev. E **91**, 012144 (2015).

[58] A. Chandran, M. D. Schulz, and F. J. Burnell, The eigenstate thermalization hypothesis in constrained Hilbert spaces: A case study in non-Abelian anyon chains, Phys. Rev. B **94**, 235122 (2016).

[59] R. Mondaini and M. Rigol, Eigenstate thermalization in the two-dimensional transverse field Ising model. II. Off-diagonal matrix elements of observables, Phys. Rev. E **96**, 012157 (2017).

[60] Z. Lan and S. Powell, Eigenstate thermalization hypothesis in quantum dimer models, Phys. Rev. B **96**, 115140 (2017).

[61] R. Hamazaki and M. Ueda, Random-matrix behavior of quantum nonintegrable many-body systems with dyson's three symmetries, Phys. Rev. E **99**, 042116 (2019).

[62] S. Goldstein, J. L. Lebowitz, R. Tumulka, and N. Zanghì, Long-time behavior of macroscopic quantum systems, Eur. Phys. J. H **35**, 173 (2010).

[63] P. Reimann, Generalization of von Neumann's Approach to Thermalization, Phys. Rev. Lett. **115**, 010403 (2015).

[64] G. P. Brandino, A. De Luca, R. M. Konik, and G. Mussardo, Quench dynamics in randomly generated extended quantum models, Phys. Rev. B **85**, 214435 (2012).

[65] P. Reimann, Eigenstate thermalization: Deutsch's approach and beyond, New J. Phys. **17**, 055025 (2015).

[66] K. Mon and J. French, Statistical properties of many-particle spectra, Ann. Phys. (N.Y.) **95**, 90 (1975).

[67] V. K. Kota, Embedded random matrix ensembles for complexity and chaos in finite interacting particle systems, Phys. Rep. **347**, 223 (2001).

[68] L. Benet and H. A. Weidenmüller, Review of the k-body embedded ensembles of Gaussian random matrices, J. Phys. A **36**, 3569 (2003).

[69] R. Hamazaki and M. Ueda, Atypicality of Most Few-Body Observables, Phys. Rev. Lett. **120**, 080603 (2018).

[70] Because the probabilistic measure P we introduce on the ensemble $\mathcal{G}^{(\alpha)}$ does not depend on the choice of an orthonormal operator basis $\{\hat{\sigma}^{(p)}\}$, we can arbitrarily choose it.

[71] See Supplemental Material at http://link.aps.org/supplemental/10.1103/PhysRevLett.129.030602, which includes Refs. [72–75], for the proof of the translation and parity symmetry of the operator defined in Eq. (3), the system size dependence of $\mathbb{E}_N[\Delta_\infty]$ for odd N, the estimation of the statistical error in Fig. 1, dynamics of our model from relatively simple initial states, the additional data for the validity of the first part of Srednicki's ansatz for $0.5 \le \alpha \le 2.0$, and the validity of the second part of Srednicki's ansatz (i.e., the distribution of $\delta O_{\gamma\gamma}$).

[72] B. Efron and R. J. Tibshirani, *An Introduction to the Bootstrap* (Chapman & Hall/CRC, London, 1994), 10.1201/9780429246593.

[73] V. Bapst and G. Semerjian, On quantum mean-field models and their quantum annealing, J. Stat. Mech. 06 (2012) P06007.

[74] J. H. Wedderburn, On hypercomplex numbers, Proc. Math. Soc. **2**, 77 (1908).

[75] O. Kabernik, Reductions in finite-dimensional quantum mechanics: from symmetries to operator algebras and beyond, Ph.D. thesis, University of British Columbia, 2021, 10.14288/1.0396110.

[76] On the other hand, it is not invariant under time-reversal operation because it contains terms like $\hat{\sigma}_j^x \hat{\sigma}_k^y$.

[77] This measure is invariant under any change of the local orthonormal operator basis $\{\hat{\sigma}^{(p)}\}_{p=0}^{d_L^2-1}$.

[78] Indeed, the asymptotic N dependence of Gaussian random matrices, Eq. (4), with fit parameters C, N_m, and N_0 fits quite well to the numerical data, including those for $\alpha = 0$ where the strong ETH typically breaks down (see Supplemental Material [71]).

[79] The ensemble average $\mathbb{E}_N[\Delta_\infty]$ shows even-odd staggered behavior as a function of N. While the reason for this behavior is unclear, we find that $\mathbb{E}_N[\Delta_\infty]$ exhibits monotonic behavior when we focus only on either odd or even N. Figure 1 shows the data for even N. The data for odd N is provided in the Supplemental Material [71].

[80] V. Oganesyan and D. A. Huse, Localization of interacting fermions at high temperature, Phys. Rev. B **75**, 155111 (2007).

[81] Y. Y. Atas, E. Bogomolny, O. Giraud, and G. Roux, Distribution of the Ratio of Consecutive Level Spacings in Random Matrix Ensembles, Phys. Rev. Lett. **110**, 084101 (2013).

[82] A. Russomanno, M. Fava, and M. Heyl, Quantum chaos and ensemble inequivalence of quantum long-range Ising chains, Phys. Rev. B **104**, 094309 (2021).

[83] A. Bäcker, M. Haque, and I. M. Khaymovich, Multifractal dimensions for random matrices, chaotic quantum maps, and many-body systems, Phys. Rev. E **100**, 032117 (2019).

[84] In the numerical calculation of $\{|E_\beta^{(0)}\rangle\}_\beta$, we take $\alpha = 0.0001$ to break the degeneracies. This value is small enough compared with the system size of the simulation and essentially describes the physics of the fully connected case ($\alpha = 0$).

[85] For Gaussian random matrices, the ensemble average of the fractal dimension D_q satisfies $\mathbb{E}[D_q] \simeq 1 - f_q/\log d$, where f_q is a constant ($f_q \simeq \log(q!)/(q-1)$ for GUE) [83].

[86] Thus, $\mathcal{S}[\delta O_{\alpha\alpha}]$ decreases exponentially with the system size when Srednicki's ansatz holds true. On the other hand, for integrable systems, where Srednicki's ansatz does not hold, $\mathcal{S}[\delta O_{\alpha\alpha}]$ is known to decrease polynomially with increasing the system size [37,87–95].

[87] A. C. Cassidy, C. W. Clark, and M. Rigol, Generalized Thermalization in an Integrable Lattice System, Phys. Rev. Lett. **106**, 140405 (2011).

[88] K. He, L. F. Santos, T. M. Wright, and M. Rigol, Single-particle and many-body analyses of a quasiperiodic integrable system after a quench, Phys. Rev. A **87**, 063637 (2013).

[89] T. N. Ikeda, Y. Watanabe, and M. Ueda, Finite-size scaling analysis of the eigenstate thermalization hypothesis in a one-dimensional interacting Bose gas, Phys. Rev. E **87**, 012125 (2013).

[90] V. Alba, Eigenstate thermalization hypothesis and integrability in quantum spin chains, Phys. Rev. B **91**, 155123 (2015).
[91] L. Vidmar and M. Rigol, Generalized Gibbs ensemble in integrable lattice models, J. Stat. Mech. 06 (2016) 064007.
[92] S. Nandy, A. Sen, A. Das, and A. Dhar, Eigenstate Gibbs ensemble in integrable quantum systems, Phys. Rev. B **94**, 245131 (2016).
[93] J. M. Magán, Random Free Fermions: An Analytical Example of Eigenstate Thermalization, Phys. Rev. Lett. **116**, 030401 (2016).
[94] M. Haque and P. A. McClarty, Eigenstate thermalization scaling in Majorana clusters: From chaotic to integrable Sachdev-Ye-Kitaev models, Phys. Rev. B **100**, 115122 (2019).
[95] M. Mierzejewski and L. Vidmar, Quantitative Impact of Integrals of Motion on the Eigenstate Thermalization Hypothesis, Phys. Rev. Lett. **124**, 040603 (2020).
[96] S. Tomov, J. Dongarra, and M. Baboulin, Towards dense linear algebra for hybrid GPU accelerated manycore systems, Parallel Comput. **36**, 232 (2010).
[97] S. Tomov, R. Nath, H. Ltaief, and J. Dongarra, Dense linear algebra solvers for multicore with GPU accelerators, *Proc. of the IEEE IPDPS'10* (IEEE Computer Society, 2010), pp. 1–8, 10.1109/IPDPSW.2010.5470941.
[98] J. Dongarra, M. Gates, A. Haidar, J. Kurzak, P. Luszczek, S. Tomov, and I. Yamazaki, Accelerating numerical dense linear algebra calculations with GPUs, Num. Comput. GPUs 1 (2014).